Heliyon 9 (2023) e16731

Contents lists available at ScienceDirect

Heliyon

journal homepage: www.cell.com/heliyon

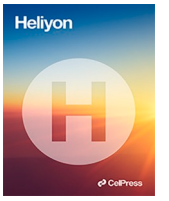

An improved microscopic traffic model for heterogeneous vehicles using the vehicle's mass effect

Zehua Si [a,*], Md Anowar Hossain [a], Jun Tanimoto [a,b]

[a] Interdisciplinary Graduate School of Engineering Sciences, Kyushu University, Kasuga-koen, Kasuga-shi, Fukuoka, 816-8580, Japan
[b] Kyushu University, Kasuga-koen, Kasuga-shi, Fukuoka, 816-8580, Japan

ARTICLE INFO

PACS:
89.40.-a (Transportation)
87.15. Aa (Theory and modeling
Computer simulation)

Keywords:
Car-following modelling
Mass effect
Time delay effect
Stability condition
mKdV equation
Traffic jam

ABSTRACT

This study aims to develop a traffic model for heterogeneous vehicle movement, which introduces the vehicle's heterogeneity by considering the internal mass effect. We explore the behavioral characteristics of the flow field generated by the proposed model and provide a comparative analysis of the conventional model. A linear stability condition is deduced to showcase the model's capacity to neutralize flow. Nonlinear analysis is employed to derive the modified Korteweg-de Vries (mKdV) equation and its corresponding analytical solution, enabling the observation of traffic flow behavior in proximity to the neutral stability condition. A numerical simulation is then conducted, considering cyclic boundary conditions. The results indicate that the mass effect tends to absorb traffic jams provided no time delay is imposed.

1. Introduction

Modern civilization now has more needs for mass transport networks as a result of the economy's rapid growth. Many researchers have proposed various traffic models to reveal the underlying fundamental mechanisms. These models can commonly be categorized into two distinct types [1]. The first type is known as the macroscopic or continuum model, which likens traffic flow to a compressible fluid and is investigated using fluid dynamics principles [2,3,4,5,6,7,8,9]. Conversely, the second type is the microscopic or ultra-discrete model, which delves into the interactions between individual vehicles as well as their relationship with the road infrastructure [10–13]. In general, microscopic rather than macroscopic models are given more consideration in this field, and the car-following model is their research hotspot. The car-following model assumes a lead vehicle followed by a subsequent one within a designated single lane, maintaining a minimum space and time gap between them [14–20]. To better mimic actual traffic flow, several improved car-following model variants have been proposed, including gas kinetic, hydrodynamic lattice, optimum velocity (OV), generalized force (GF), and full velocity difference (FVD) models [21–27].

All vehicles are supposed to maintain the same driving behavior in most car-following traffic models, yet the actual situations are difficult to represent. In actual traffic scenarios, the car-following behaviors exhibit heterogeneity due to varying conditions of drivers or vehicles [28–38]. One of the most typical examples is that vehicles vary in size. Lighter vehicles, like compact cars, have a low mass, resulting in low inertia, enabling them to accelerate or decelerate easily. Consequently, drivers of such vehicles frequently alter their driving behavior to optimize traffic efficiency. In contrast, heavier vehicles, such as trucks, have a greater mass, leading to higher

* Corresponding author.
E-mail address: si.zehua.328@s.kyushu-u.ac.jp (Z. Si).

https://doi.org/10.1016/j.heliyon.2023.e16731
Received 8 March 2023; Received in revised form 25 May 2023; Accepted 25 May 2023
Available online 29 May 2023

inertia and making it difficult to accelerate or decelerate quickly. To maintain safety, drivers of heavy vehicles tend to preserve their driving behavior. The distinctions in driving behavior are widespread in traffic flow systems and have far-reaching effects, which has motivated us to improve conventional car-following models by considering this factor.

The driver needs reaction time from receiving environmental stimuli to responding to the actual driving process. It may also take a mechanical response time for a vehicle to adjust to the expected speed after the driver's operation. Time delay caused by these two cases in the traffic flow system has been considered by Chandler et al. [39] and incorporated into the OV model by Bando and her colleagues [40]. In line with these pioneering studies, many researchers have accounted for the time delay effect in the traffic flow models. They clarified that this impacts traffic flow systems' stability [41–45]. Because of this, the proposed model also considers the time delay effect to explore its impact on heterogeneous traffic flow systems besides the effect of mass as mentioned.

Based on the above, this study improved the conventional car-following model by incorporating the mass effect factor (M_f) to account for the vehicle's mass effect. To achieve this, vehicles are divided into three types according to the M_f value for simplicity: heavy mass vehicle (HV), medium mass vehicle (MV), and light mass vehicle (LV). We study the traffic flow by varying the proportions of these three types of vehicles with or without time delay considerations.

The subsequent sections of this paper are structured as follows: Section 2 presents an overview of conventional traffic flow models. Section 3 provides a detailed explanation of the proposed model. In Section 4, a linear stability analysis of the model is conducted, while its nonlinear analysis is discussed in Section 5. The numerical simulation results are presented in Section 6. Finally, Section 7 outlines the main findings obtained from this study.

2. Background of car-following models

In 1995, a groundbreaking model called the OV model was proposed by Bando et al. [46], bringing about a remarkable advancement in the field of traffic flow analysis. The OV model's dynamic equation can be described in Eq. (1):

$$\frac{dv_n(t)}{dt} = a[V[\Delta x_n(t)] - v_n(t)] \tag{1}$$

The velocity of vehicle n at time t is denoted as $v_n(t)$, while its position is represented by $x_n(t)$. The sensitivity effect factor of the driver is indicated by a. The headway between vehicle $n+1$ and vehicle n at time t is calculated as $\Delta x_n = x_{n+1} - x_n$. The optimal velocity function, denoted as $V(\bullet)$, is adopted in the following manner:

$$V(\Delta x_n(t)) = \frac{v_{max}}{2}[\tanh(\Delta x_n(t) - h_c) + \tanh(h_c)], \tag{2}$$

While the OV model successfully simulates certain aspects of traffic flow, such as the propagation of traffic jams and stop-and-go waves, it falls short of accurately replicating realistic acceleration and deceleration. To address this limitation, Helbing and Tilch [47] introduced the GF model, an improved car-following model that takes into account negative speed differences. The GF model's governing equation is presented in Eq. (3):

$$\frac{dv_n(t)}{dt} = a[V[\Delta x_n(t)] - v_n(t)] + \lambda \Delta v_n(t) H(-v_n(t)), \tag{3}$$

The GF model incorporates the Heaviside function H, where λ represents the sensitivity effect factor (distinct from a). At time t, the velocity difference $\Delta v_n(t)$ between vehicle $n+1$ and vehicle n is defined as the disparity between their velocities, v_{n+1} and v_n. The results indicate that the GF model demonstrates a closer alignment with the observed field data compared to the OV model.

Based on the GF model, Jiang et al. [48] conducted a study in 2001 and revealed the significant impact of both positive and negative velocity differences on traffic flow stability. Furthermore, they proposed the Full Velocity Difference (FVD) model to address this issue:

$$\frac{dv_n(t)}{dt} = a[V[\Delta x_n(t)] - v_n(t)] + \lambda \Delta v_n(t), \tag{4}$$

The FVD model described in Eq. (4) has been considered the standard form of the car-following model because of its conciseness and practicality. We also consider it a benchmark, and the next section will discuss the details.

3. Proposed model

Following the FVD model, we proposed a heterogeneous vehicular mass (HVM) model by considering the vehicle's mass and time delay effects. Its dynamics equation is as follows:

$$\frac{dv_n(t)}{dt} = a[V[\Delta x_n(t-\tau)] - v_n(t)] + \lambda \Delta v_n(t), \tag{5}$$

The dynamics equation incorporates a time delay factor, denoted as τ, which encompasses the time delay effect originating from the response time of vehicles' mechanical operation and drivers' reaction to stimuli. The mass effect of the vehicle is manifested through the adoption of the optimal velocity function, represented as follows:

$$V(\Delta x_n(t)) = \frac{v_{max}}{2}\left[\tanh\left(M_f(\Delta x_n(t) - h_c)\right) + \tanh(h_c)\right], \tag{6}$$

where M_f denotes the mass effect factor, v_{max} represents the maximum velocity, and h_c denotes the safety distance. Due to the non-existence of a vehicle with negative or no mass in real life, the value of M_f should be positive. Vehicles have heavy mass when $0 < M_f < 1$, limiting them to changing their driving behavior frequently. When $M_f > 1$, the vehicles' light mass allows them to accelerate or decelerate quickly. When $M_f = 1$, Eq. (6) conforms to the optimal velocity function Eq. (2) adopted the OV model, which means only medium mass vehicles are considered. To simplify the analysis, we assign fixed values of 0.75, 1.00, and 1.50 to M_f for HV, MV, and LV, respectively. A comparison between their respective OV function diagrams and the conventional OV model illustrated in Fig. 1.

One notable observation from Fig. 1 is that the velocity curve of LV exhibits the steepest slope when the headway falls within a reasonable range. In comparison, MV demonstrates a relatively smaller slope, while HV exhibits the smallest slope. The result indicates that under the same headway from the preceding vehicle, the lighter LV can adjust its velocity to the expected value more quickly due to its smaller inertia, while the heavier MV and HV require more time to adjust their velocities due to their larger inertia. This phenomenon is consistent with our assumptions and also conforms to reality.

It should be mentioned that although our model deals with heterogeneous traffic flow systems, in which heavy mass, medium mass, and light mass vehicles coexist simultaneously. But for theoretical analysis, we restrict our model to a homogeneous microscopic perspective in the following *Linear Stability Analysis* and *Nonlinear Analysis* sections. In the *Numerical Simulations* section, we return to the heterogeneous microscopic model and investigate several typical mixed traffic flows composed of different mass vehicles.

4. Linear stability analysis

To determine the stability of the steady flow state in the HVM model outlined in Eq. (5) along with Eq. (6), a linear stability analysis is performed. In this analysis, we make the assumption that all vehicles move in a linear formation, maintaining a consistent headway represented as b, while adhering to the optimal velocity denoted as $V(b)$. Consequently, in the case of uniform traffic flow, the solution for Eq. (5) can be expressed as follows:

$$x_n^0(t) = b \bullet n + V(b) \bullet t \quad \text{and} \quad b = L/N, \tag{7}$$

where N represents the number of vehicles and L corresponds to the road length.

Let us present a perturbed solution for the case of $y_n(t)$, which is a slight deviation from the steady-state solution $x_n^0(t)$:

$$x_n(t) = x_n^0(t) + y_n(t), \tag{8}$$

By substituting Eqs. (7) and (8) into Eq. (5), we derive the linearized form of the model as follows:

$$\frac{dv_n(t)}{dt} = a\left[V'(b)\Delta y_n(t-\tau) - \frac{dy_n(t)}{dt}\right] + \lambda\frac{d\Delta y_n(t)}{dt}, \tag{9}$$

Where $\Delta y_n(t) = y_{n+1}(t) - y_n(t)$ and $V'(b) = \frac{dV(\Delta x_n)}{d\Delta x_n}\Big|_{\Delta x_n = b}$. By expanding $y_n(t) \propto exp(ikn + zt)$, the following equation of z is obtained from Eq. (9).

$$z^2 = a\left[V'(b)e^{-z\tau}\left(e^{ik} - 1\right) - z\right] + \lambda z\left(e^{ik} - 1\right), \tag{10}$$

Suppose that $z = z_1(ik) + z_2(ik)^2 + \cdots$. Substituting this expression into Eq. (10), we can determine the first- and second-order components of ik are as in Eq. (11):

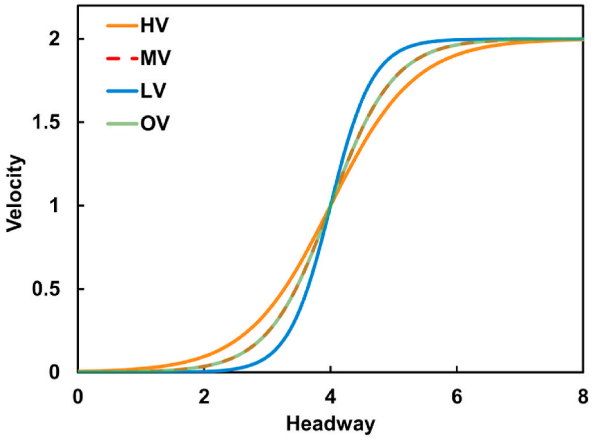

Fig. 1. The optimal velocity profiles for different vehicle types are determined based on their mass effect factors M_f: 0.75 for heavy mass vehicles (HV), 1.00 for medium mass vehicles (MV), and 1.50 for light mass vehicles (LV), along with the conventional OV function.

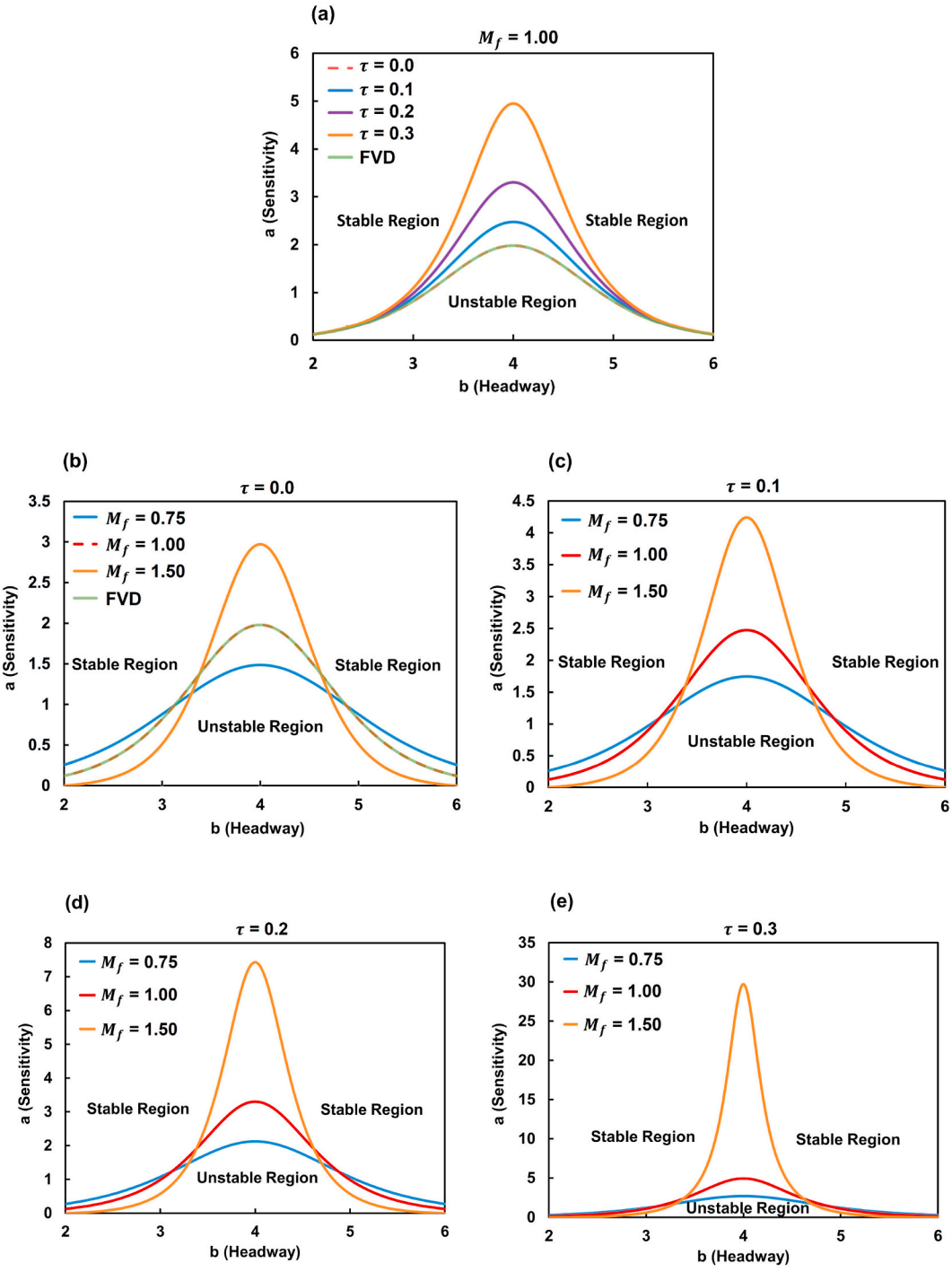

Fig. 2. Headway-sensitivity phase diagrams (b, a) with $\lambda = 0.1$. In Panel (a), a comparison is made between the results obtained from the FVD model and the HVM model. The mass effect factor M_f is held constant at 1.00, while the time delay effect τ varies across values of 0.0, 0.1, 0.2, and 0.5. Panels (b) to (e) illustrate the comparison of results obtained from the HVM model with different values of M_f, while the time delay effect τ is fixed at 0.0, 0.1, 0.2, and 0.3, respectively.

$$z_1 = V'(b), z_2 = V'(b)\left[\frac{1}{2}+\frac{\lambda}{a}-V'(b)\left(\tau+\frac{1}{a}\right)\right], \tag{11}$$

Assume the condition presented in Eq. (12) is met, in such case, even a minor disturbance input will cause the traffic flow to become unstable.

$$a < \frac{2[V'(b)-\lambda]}{1-2\tau V'(b)}, \tag{12}$$

Therefore, the proposed model's linear stability condition can be stated as follows:

$$a = \frac{2[V'(b)-\lambda]}{1-2\tau V'(b)}. \tag{13}$$

It is worth pointing out that although the linear stability condition of our proposed model given by Eq. (6) is formally consistent with the previous time-delay models, the $V'(\bullet)$ in them are completely different because we have adopted a different optimal velocity function $V(\bullet)$.

Fig. 2 illustrates the proposed model's flow stability states per the neutral stability condition described in Eq. (13). Fig. 2 (a) confirms that increasing time delay would destroy stability. At the limit, the proposed model fully recovers the conventional FVD model assuming $\tau = 0$. It is conceivable that any delay, be it due to the response time of a vehicle's mechanical operation or the driver's reaction, ultimately contributes to undesirable disturbances to the overall dynamic traffic flow system. The comparison of panels (b) to (e) in Fig. 2 supports this observation, where a more significant time delay leads to a substantial increase in unstable regions. Referring to Fig. 2 (b), it can be seen that the stability region expands as M_f decreases. This is due to the infrequency of acceleration or deceleration in vehicles with heavier mass, thus a smaller M_f value promotes flow field stabilization.

5. Nonlinear analysis

We utilize the reductive perturbation method outlined in Refs. [49,50] to obtain the modified Korteweg-de Vries (mKdV) equation, capable of representing the density wave of kink-antikink near the critical point in the HVM model.

Firstly, we rewrite Eq. (5) into the form of headway:

$$\frac{d^2(\Delta x_n(t))}{dt^2} = a\left[\{V[\Delta x_{n+1}(t-\tau)] - V[\Delta x_n(t-\tau)]\} - \frac{d\Delta x_n(t)}{dt}\right] + \lambda\left[\frac{d\Delta x_{n+1}(t)}{dt} - \frac{d\Delta x_n(t)}{dt}\right], \tag{14}$$

In the unstable traffic flow region, we introduced a small positive parameter ε in proximity to the critical point (a_c, h_c), defining the slow-scale variables X and T [51,52]. Consequently, these variables undergo the following transformation:

$$X = \varepsilon(n+bt) \text{ and } T = \varepsilon^3 t \text{ with } 0 < \varepsilon \ll 1, \tag{15}$$

where b represents a predetermined constant, the expression for the headway can be stated as follows:

$$\Delta x_n(t) = h_c + \varepsilon R(X,T), \tag{16}$$

The nonlinear partial differential equation, which arises from the expansion of Eq. (14) to the fifth order of ε with the inclusion of Eq. (15) and Eq. (16), can be expressed as follows:

$$\begin{aligned}\varepsilon^2[b-V'(h_c)]\partial_X R + \varepsilon^3\left[\frac{b^2-\lambda b}{a} - \frac{(1-2b\tau)}{2}V'(h_c)\right]\partial_X^2 R + \varepsilon^4\left[\partial_T R - \left(\frac{(b\tau)^3+(1-b\tau)^3}{6}V'(h_c) + \frac{\lambda b^2}{a}\right)\partial_X^3 R - \frac{1}{2}V'''(h_c)\partial_X R^3\right] \\ + \varepsilon^5\left[\left(\frac{\lambda-2b}{a} - \tau V'(h_c)\right)\partial_X^2 R + \left(\frac{(b\tau)^4-(1-b\tau)^4}{24}V'(h_c) - \frac{\lambda b^3}{a}\right)\partial_X^4 R + \frac{(2b\tau-1)}{4}V'''(h_c)\partial_X^2 R^3\right] = 0,\end{aligned} \tag{17}$$

where $V'(h_c) = \frac{dV(\Delta x_n(t-\tau))}{d\Delta x_n(t-\tau)}\Big|_{\Delta x_n(t-\tau)=b}$ and $V'''(h_c) = \frac{d^3V(\Delta x_n(t-\tau))}{d(\Delta x_n(t-\tau))^3}\Big|_{\Delta x_n(t-\tau)=b}$.

Table 1
The effect factors g_i of the proposed model.

g_1	$= \frac{(b\tau)^3+(1-b\tau)^3}{6}V'(h_c) + \frac{\lambda b^2}{a}$
g_2	$= -\frac{1}{2}V'''(h_c)$
g_3	$= \frac{\lambda-2b}{a} - \tau V'(h_c)$
g_4	$= \frac{(b\tau)^4-(1-b\tau)^4}{24}V'(h_c) - \frac{\lambda b^3}{a}$
g_5	$= \frac{(2b\tau-1)}{4}V'''(h_c)$

Suppose $a_c = a(1+\varepsilon^2)$ and $b = V'$ near the critical point (a_c, h_c), if we neglect the second- and third-order terms of ε in Eq. (17), we obtain Eq. (18) in the following manner:

$$\varepsilon^4\left(\partial_T R - g_1\partial_X^3 R + g_2\partial_X R^3\right) + \varepsilon^5\left(g_3\partial_X^2 R + g_4\partial_X^2 R^3 + g_5\partial_X^4 R\right) = 0, \tag{18}$$

The values of g_i can be found in Table 1.

We obtain the modified Korteweg-de Vries (mKdV) equation with higher-order correction through the application of the subsequent transformations:

$$T = \frac{1}{g_1}T' \quad \text{and} \quad R = \sqrt{\frac{g_1}{g_2}}R', \tag{19}$$

Therefore, we derive the standard mKdV equation incorporating additional terms of higher-order corrections.

$$\partial_{T'}R' - \partial_X^3 R'^3 + \partial_X R'^3 + \varepsilon M[R'] = 0, \tag{20}$$

where $M[R'] = \frac{1}{g_1}\left[g_3\partial_X^2 R' + g_4\partial_X^4 R' + \frac{g_1 g_5}{g_2}\partial_X^2 R'^3\right]$.

By neglecting the perturbed term $O(\varepsilon)$ from Eq. (20), the kink–antikink wave solution of the mKdV equation is obtained, given by the following expression:

$$R_0'(X, T') = \sqrt{c}\tanh\left[\sqrt{\frac{c}{2}}(X - cT')\right], \tag{21}$$

The amplitude, c, of the kink-antikink solutions of the mKdV equation in Eq. (21) is a free parameter. The condition for choosing a particular member of the continuous family of mKdV solitons [51,52] is provided by the perturbed term $O(\varepsilon)$ in Eq. (20). For the kink-antikink solutions, by applying the solvability condition described in Eq. (22), we can determine the value of c:

$$\left(R_0', M[R']\right) = \int_{-\infty}^{\infty} dX R_0' M\left[R_0'\right] = 0, \tag{22}$$

where $M[R_0'] = M[R']$. Thus, the propagation velocity c for the kink–antikink soliton solution is determined as shown in Eq. (23):

$$c = \frac{5g_2g_3}{2g_2g_4 - 3g_1g_5}, \tag{23}$$

Therefore, by inserting Eq. (19) into Eq. (21), we derived the expression for the kink–antikink wave solution of the mKdV equation, which can be written as presented in Eq. (24):

$$R(X, T) = \sqrt{\frac{g_1 c}{g_2}}\tanh\left[\sqrt{\frac{c}{2}}(X - cg_1T)\right] \tag{24}$$

Hence, the ordinary form for the kink-antikink wave solution of the headway outlined in Eq. (14) can be expressed as shown in Eq. (25):

$$\Delta x_n = h_c + \sqrt{\frac{g_1 c}{g_2}\left(\frac{a_c}{a} - 1\right)}\tanh\sqrt{\frac{c}{2}\left(\frac{a_c}{a} - 1\right)}\left[n + \left(1 - cg_1\left(\frac{a_c}{a} - 1\right)t\right)\right]. \tag{25}$$

Thus, we derived the amplitude A of the kink–antikink soliton solution as presented in Eq. (26):

$$A = \sqrt{\frac{g_1 c}{g_2}\left(\frac{a_c}{a} - 1\right)}. \tag{26}$$

The presence of the coexisting flow phase is characterized by the kink–antikink wave solution. In the scenario of low traffic density, the free-flow phase can be represented by $\Delta x_n = h_c + A$, while the congested flow phase is indicated by $\Delta x_n = h_c - A$ under higher traffic density.

6. Numerical simulations

In a real traffic flow system, vehicles are heterogeneous, unlike previous models, which presume that a vehicle's car-following behavior is the same. The most advantageous point of the present model is that each of the vehicles has one of three different mass effects, which implies that the proposed model can reproduce a mixed flow situation if HV, MV, and LV coexist.

We conduct several numerical simulations with the initial perturbations under periodic (cyclic) boundary conditions as shown in Eq. (27) to validate the theoretical results [53]:

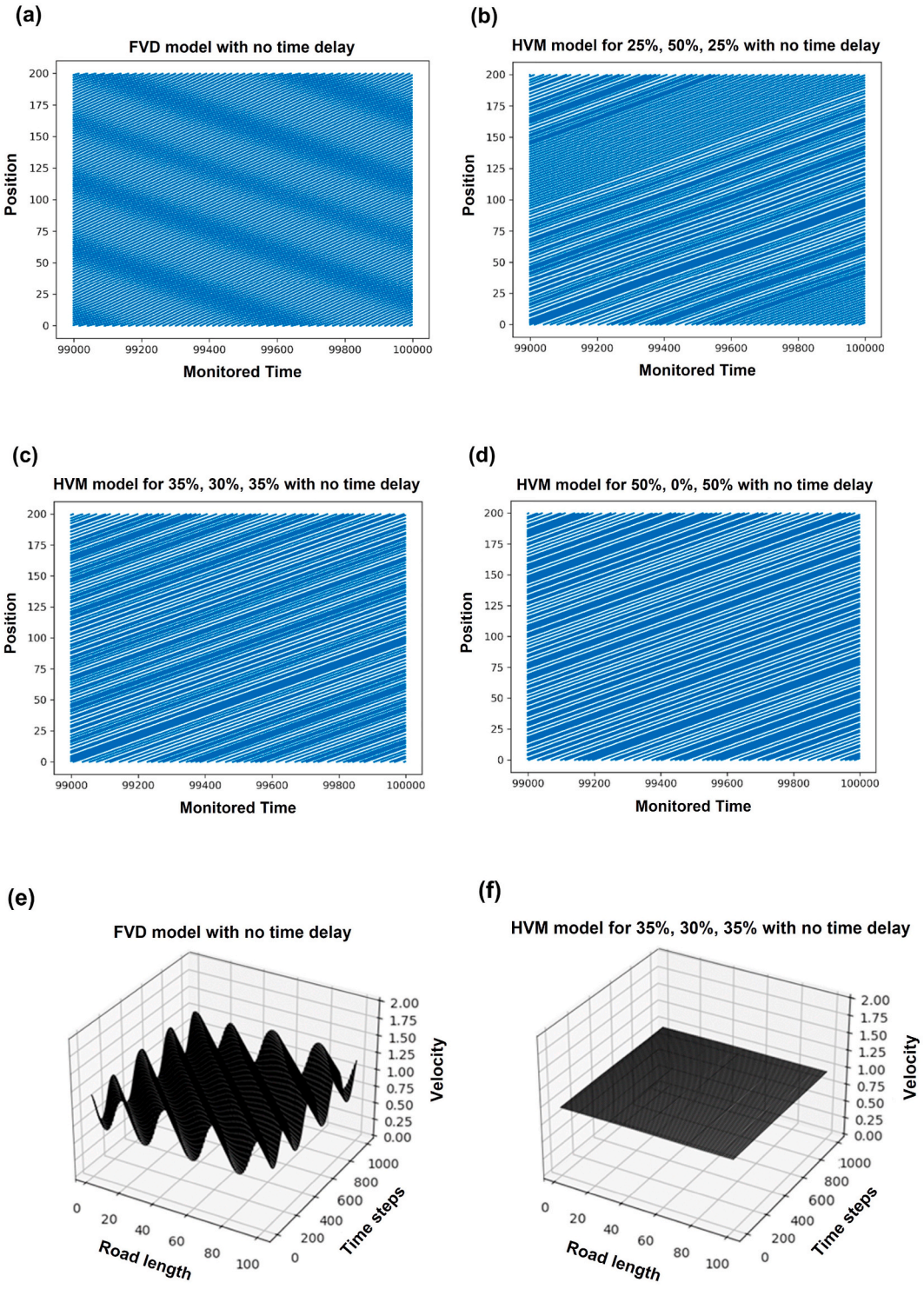

Fig. 3. Comparison of the spatiotemporal diagrams between the FVD and HVM models without a time delay effect. Panel (a) refers to the position–time spatiotemporal diagrams of FVD, and panels (b)–(d) refer to that of the HVM model in which the proportions of heavy mass vehicles (HV), medium mass vehicles (MV), and light mass vehicles (LV) are (b) 25%, 50%, 25%; (c) 35%, 30%, 35%; (d) 50%, 0%, 50%, respectively. Panels (e) and (f) refer to the spatiotemporal structure of velocity using the FVD and HVM models. The HVM model presumes that the proportions of HV, MV, and LV are 35%, 30%, and 35%.

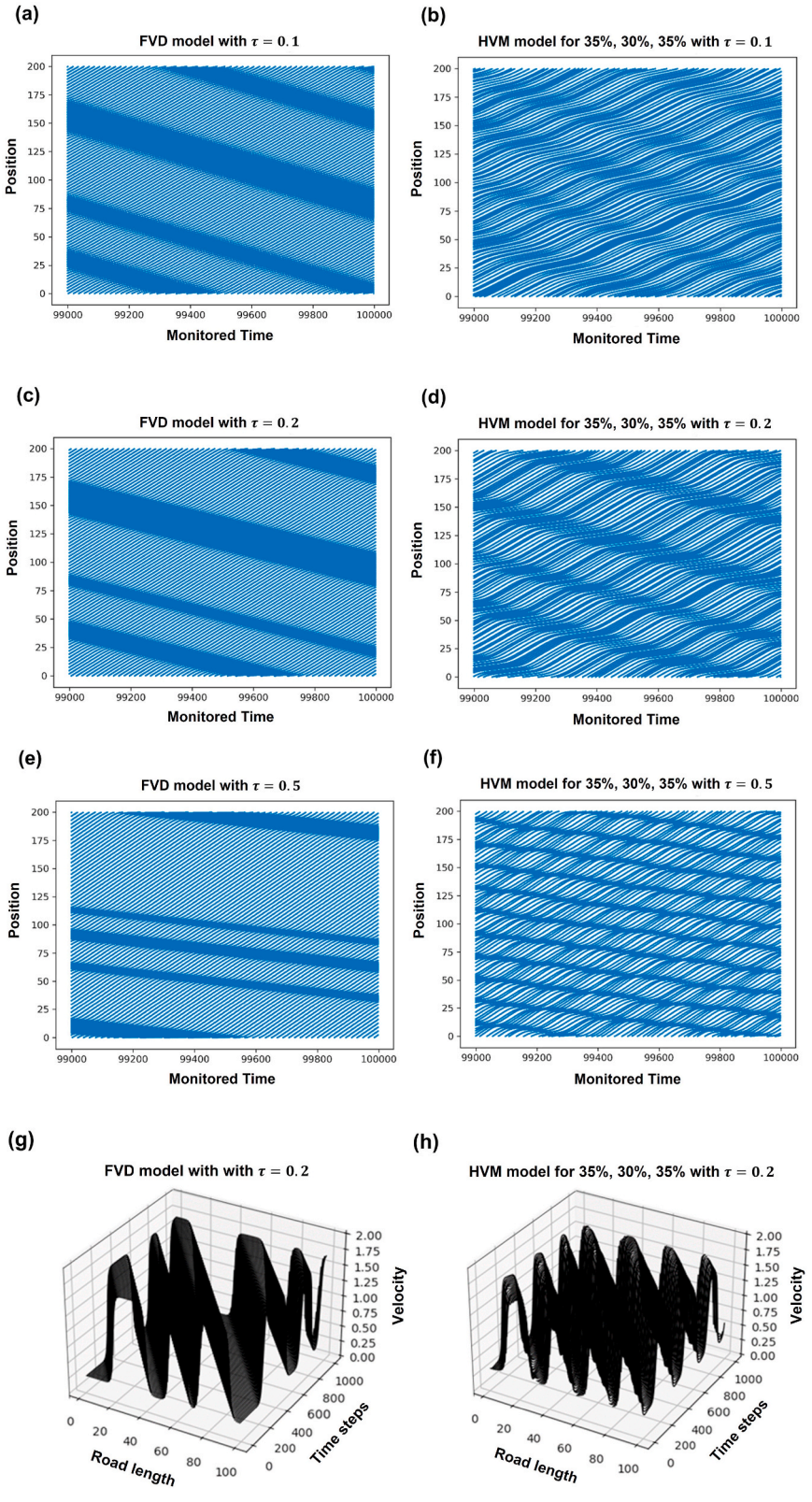

(caption on next page)

Fig. 4. Comparison of the spatiotemporal diagrams between the FVD and HVM models with the time delay effect τ. Panels (a)–(f) compare the position-time spatiotemporal diagrams of the FVD and HVM model, in which the proportions of HV, MV, and LV are 35%, 30%, and 35%. The time delay effect τ varies with 0.1 ((a) and (b)), 0.2((c) and (d)) and 0.5 ((e) and (f)). Panels (g) and (h) refer to the spatiotemporal velocity structure using the FVD and HVM models with a time delay effect τ of 0.2. The HVM model presumes that the proportions of HV, MV, and LV are 35%, 30%, and 35%.

$$\begin{cases} \Delta x_n(0) = \Delta x_n(1) = \Delta x_0 = \dfrac{L}{N}, \text{for } n \neq \dfrac{N}{2}, \dfrac{N}{2}+1 \\ \Delta x_n(0) = \Delta x_0 + 0.5, \text{for } n = \dfrac{N}{2} \\ \Delta x_n(0) = \Delta x_0 - 0.5, \text{for } n = \dfrac{N}{2}+1 \end{cases} \tag{27}$$

where Δx_0 denotes the average headway. Other parameters are assumed as follows: the total number of vehicles was $N = 100$, the road length was $L = 200$, the sensitivity was $a = 1$ and $b = L/N$. The vehicles' order, either HV, MV, or LV, is presumed random, whereas the fractions of those three classes are systematically varied in a series of simulations.

Without considering the time delay effect, panels (a) to (d) in Fig. 3 compare the spatiotemporal diagrams between the conventional FVD model and the proposed model. To make the figure as representative as possible, the diagrams are taken between the time steps of t = 99,000 to t = 100,000, where the whole traffic system is inclined to stabilize after sufficient time evolution. The proportions of HV, MV, and LV in the proposed model are fixed as (25%, 50%, 25%), (35%, 30%, 35%), and (50%, 0%, 50%) in Fig. 3 (b) to (d), respectively. Note that the fraction of HV is kept the same as that of LV to compare it with a homogeneous traffic flow system using the conventional FVD. Fig. 3 (a), produced using the FVD, exhibits several heavy traffic jam areas. However, the phenomenon predicted by the HVM model is entirely different. As shown in panels (b) to (d) in Fig. 3, although the vehicle's trajectories oscillate, the traffic jam areas disappear. The spatiotemporal velocity structures using those two models show this difference more explicitly. One can observe that the FVD model was agitated with stop-and-go waves in Fig. 3 (e), whereas in Fig. 3 (f), the HVM model yields a stable and middle-velocity extent.

Fig. 4 presents the comparisons concerning the spatiotemporal diagrams between the conventional FVD model and the proposed model, where the time delay effect is further implemented to the mass effect. The fractions of the HV, MV, and LV in the HVM model were fixed at (35%, 30%, 35%), whereas the time delay factor: τ, was varied as 0.1 (top row), 0.2 (second row), and 0.5 (bottom row), respectively. The other parameters are set similar to those in Fig. 3. Note that the HVM model with a time delay would inevitably suffer from traffic jams, unlike that without a time delay (Fig. 3). With time delay increase, especially in the case of $\tau = 0.5$, the HVM model produces spatially-frequent stop-and-go waves (panel (f) in Fig. 4) vis-à-vis what the FVD model predict (panel (e) in Fig. 4). Interestingly, amid two neighboring stop-and-go waves, the HVM model shows slight meandering trajectories of freely running vehicles (panels (b), (d), and (f) in Fig. 4). Whereas the FVD (panels (a), (c), and (e) in Fig. 4) does not show such a tendency. The such visual difference is attributed to whether heterogeneity or homogeneity is considered in a traffic flow field.

7. Conclusion and discussion

Based on the FVD model, this paper proposed an improved car-following model called the HVM model, which can highlight the mass and time delay effects. We introduced the mass effect factor (M_f) into an OV function and divided vehicles into three classes according to their mass effect factor value to reproduce a mixed flow system that might be more realistic than the predictions of conventional homogeneous models.

According to the linear stability analysis, it was confirmed that the stability of the proposed model is positively correlated with the magnitude of the mass effect and inversely correlated with the impact of time delay. The nonlinear analysis drew the analytical solution as a soliton wave using the KdV–Burgers equation. The numerical results illustrate the difference between the HVM and the predictions of the conventional FVD model. This implies that the HVM could reproduce a more realistic traffic flow field because a mixed heterogeneous flow is implemented, unlike the FVD.

It is worth noting that although our numerical simulation reproduces a heterogeneous traffic flow composed of different mass vehicles, our linear stability analysis and nonlinear analysis are still based on a homogeneous microscopic model. If we extend it to the heterogeneous macroscopic model, we will be able to theoretically analyze the heterogeneous traffic flow composed of different mass vehicles, which is one of our subsequent works.

Author contribution statement

Zehua Si: Performed the experiments; Analyzed and interpreted the data; Contributed reagents, materials, analysis tools or data; Wrote the paper. Md. Anowar Hossain: Conceived and designed the experiments; Performed the experiments; Analyzed and interpreted the data; Contributed reagents, materials, analysis tools or data. Jun Tanimoto: Conceived and designed the experiments; Analyzed and interpreted the data; Contributed reagents, materials, analysis tools or data; Wrote the paper.

Data availability statement

No data was used for the research described in the article.

Declaration of competing interest

The authors declare that they have no known competing financial interests or personal relationships that could have appeared to influence the work reported in this paper.

Acknowledgments

This study was partially supported by Grant-in-Aid for Scientific Research from JSPS, Japan, KAKENHI (Grant No. JP 19KK0262, JP 20H02314 and JP 20K21062) awarded to Professor Tanimoto. We would like to express our gratitude to them.

References

[1] J. Tanimoto, Evolutionary Games with Sociophysics, 2018.
[2] T. Nagatani, Modified KdV equation for jamming transition in the continuum models of traffic, Phys. A Stat. Mech. Its Appl. 261 (1998) 599–607, https://doi.org/10.1016/S0378-4371(98)00347-1.
[3] M.A. Hossain, J. Tanimoto, The "backward-looking" effect in the continuum model considering a new backward equilibrium velocity function, Nonlinear Dynam. 106 (2021) 2061–2072, https://doi.org/10.1007/s11071-021-06894-2.
[4] H.K. Lee, H.W. Lee, D. Kim, Macroscopic traffic models from microscopic car-following models, Phys. Rev. E - Stat. Physics, Plasmas, Fluids, Relat. Interdiscip. Top. 64 (2001) 12, https://doi.org/10.1103/PhysRevE.64.056126.
[5] R. Jiang, Q.S. Wu, Z.J. Zhu, A new continuum model for traffic flow and numerical tests, Transp. Res. Part B Methodol. 36 (2002) 405–419, https://doi.org/10.1016/S0191-2615(01)00010-8.
[6] C. Zhai, W. Wu, Y. Xiao, Non-lane-discipline-based continuum model considering the effect of lateral gaps and electronic throttle dynamics, Chin. J. Phys. (2023), https://doi.org/10.1016/j.cjph.2023.03.013.
[7] C. Zhai, W. Wu, A continuum model considering the uncertain velocity of preceding vehicles on gradient highways, Phys. A Stat. Mech. Its Appl. 588 (2022), 126561, https://doi.org/10.1016/j.physa.2021.126561.
[8] C. Zhai, W. Wu, A continuous traffic flow model considering predictive headway variation and preceding vehicle's taillight effect, Phys. A Stat. Mech. Its Appl. 584 (2021), 126364, https://doi.org/10.1016/j.physa.2021.126364.
[9] C. Zhai, W. Wu, Analysis of drivers' characteristics on continuum model with traffic jerk effect, Phys. Lett. Sect. A Gen. At. Solid State Phys. 382 (2018) 3381–3392, https://doi.org/10.1016/j.physleta.2018.09.029.
[10] T. Tang, Y. Wang, X. Yang, Y. Wu, A new car-following model accounting for varying road condition, Nonlinear Dynam. 70 (2012) 1397–1405, https://doi.org/10.1007/s11071-012-0542-8.
[11] M.A. Hossain, K.M.A. Kabir, J. Tanimoto, Improved car-following model considering modified backward optimal velocity and velocity difference with backward-looking effect, J. Appl. Math. Phys. 9 (2021) 242–259, https://doi.org/10.4236/jamp.2021.92018.
[12] H.X. Ge, S.Q. Dai, L.Y. Dong, Y. Xue, Stabilization effect of traffic flow in an extended car-following model based on an intelligent transportation system application, Phys. Rev. E - Stat. Physics, Plasmas, Fluids, Relat. Interdiscip. Top. 70 (2004) 6, https://doi.org/10.1103/PhysRevE.70.066134.
[13] T. Tang, W. Shi, H. Shang, Y. Wang, A new car-following model with consideration of inter-vehicle communication, Nonlinear Dynam. 76 (2014) 2017–2023, https://doi.org/10.1007/s11071-014-1265-9.
[14] G.F. Newell, Nonlinear effects in the dynamics of car following, Oper. Res. 9 (1961) 209–229, https://doi.org/10.1287/opre.9.2.209.
[15] M.A. Hossain, J. Tanimoto, A microscopic traffic flow model for sharing information from a vehicle to vehicle by considering system time delay effect, Phys. A Stat. Mech. Its Appl. 585 (2022), 126437, https://doi.org/10.1016/j.physa.2021.126437.
[16] L. Yu, Z.K. Shi, T. Li, A new car-following model with two delays, Phys. Lett. Sect. A Gen. At. Solid State Phys. 378 (2014) 348–357, https://doi.org/10.1016/j.physleta.2013.11.030.
[17] H.X. Ge, Y. Cui, K.Q. Zhu, R.J. Cheng, The control method for the lattice hydrodynamic model, Commun. Nonlinear Sci. Numer. Simul. 22 (2015) 903–908, https://doi.org/10.1016/j.cnsns.2014.09.014.
[18] C. Zhai, W. Wu, A new car-following model considering driver's characteristics and traffic jerk, Nonlinear Dynam. 93 (2018) 2185–2199, https://doi.org/10.1007/s11071-018-4318-7.
[19] C. Zhai, W. Wu, Self-delayed feedback car-following control with the velocity uncertainty of preceding vehicles on gradient roads, Nonlinear Dynam. 106 (2021) 3379–3400, https://doi.org/10.1007/s11071-021-06970-7.
[20] C. Zhai, W. Wu, Y. Xiao, Cooperative car-following control with electronic throttle and perceived headway errors on gyroidal roads, Appl. Math. Model. 108 (2022) 770–786, https://doi.org/10.1016/j.apm.2022.04.010.
[21] K. Nagel, M. Schreckenberg, A cellular automaton model for freeway traffic, J. Phys. 2 (1992) 2221–2229, https://doi.org/10.1051/jp1:1992277.
[22] E. Fukuda, J. Tanimoto, Y. Iwamura, K. Nakamura, A. Mitsuhiro, Field measurement analysis to validate lane-changing behavior in a cellular automaton model, Phys. Rev. E. 94 (2016) 1–7, https://doi.org/10.1103/PhysRevE.94.052209.
[23] H.X. Ge, P.J. Zheng, S.M. Lo, R.J. Cheng, TDGL equation in lattice hydrodynamic model considering driver's physical delay, Nonlinear Dynam. 76 (2014) 441–445, https://doi.org/10.1007/s11071-013-1137-8.
[24] R. Jiang, M. Bin Hu, H.M. Zhang, Z.Y. Gao, B. Jia, Q.S. Wu, On some experimental features of car-following behavior and how to model them, Transp. Res. Part B Methodol. 80 (2015) 338–354, https://doi.org/10.1016/j.trb.2015.08.003.
[25] C. Zhai, W. Wu, An extended multi-phase lattice model with consideration of optimal current changes with memory, Cluster Comput. 22 (2019) 7447–7457, https://doi.org/10.1007/s10586-018-1773-3.
[26] C. Zhai, W. Wu, Y. Xiao, Q. Luo, Y. Zhang, Modeling bidirectional pedestrian flow with the perceived uncertainty of preceding pedestrian information, Phys. A Stat. Mech. Its Appl. 597 (2022), 127205, https://doi.org/10.1016/j.physa.2022.127205.
[27] C. Zhai, W. Wu, Designing continuous delay feedback control for lattice hydrodynamic model under cyber-attacks and connected vehicle environment, Commun. Nonlinear Sci. Numer. Simul. 95 (2021), 105667, https://doi.org/10.1016/j.cnsns.2020.105667.
[28] D. Yang, P. Jin, Y. Pu, B. Ran, Stability analysis of the mixed traffic flow of cars and trucks using heterogeneous optimal velocity car-following model, Phys. A Stat. Mech. Its Appl. 395 (2014) 371–383, https://doi.org/10.1016/j.physa.2013.10.017.
[29] Z. Yao, R. Hu, Y. Wang, Y. Jiang, B. Ran, Y. Chen, Stability analysis and the fundamental diagram for mixed connected automated and human-driven vehicles, Phys. A Stat. Mech. Its Appl. 533 (2019), 121931, https://doi.org/10.1016/j.physa.2019.121931.
[30] Z. Yao, Y. Wu, Y. Wang, B. Zhao, Y. Jiang, Analysis of the impact of maximum platoon size of CAVs on mixed traffic flow: an analytical and simulation method, Transport. Res. C Emerg. Technol. 147 (2023), 103989, https://doi.org/10.1016/j.trc.2022.103989.
[31] J. Wang, F. Sun, H. Ge, Effect of the driver's desire for smooth driving on the car-following model, Phys. A Stat. Mech. Its Appl. 512 (2018) 96–108, https://doi.org/10.1016/j.physa.2018.08.025.

[32] F. Sun, J. Wang, R. Cheng, H. Ge, An extended heterogeneous car-following model accounting for anticipation driving behavior and mixed maximum speeds, Phys. Lett. Sect. A Gen. At. Solid State Phys. 382 (2018) 489–498, https://doi.org/10.1016/j.physleta.2017.12.037.
[33] L. Huang, C. Zhai, H. Wang, R. Zhang, Z. Qiu, J. Wu, Cooperative Adaptive Cruise Control and exhaust emission evaluation under heterogeneous connected vehicle network environment in urban city, J. Environ. Manag. 256 (2020), 109975, https://doi.org/10.1016/j.jenvman.2019.109975.
[34] Z. Yao, R. Hu, Y. Jiang, T. Xu, Stability and safety evaluation of mixed traffic flow with connected automated vehicles on expressways, J. Saf. Res. 75 (2020) 262–274, https://doi.org/10.1016/j.jsr.2020.09.012.
[35] Z. Yao, T. Xu, Y. Jiang, R. Hu, Linear stability analysis of heterogeneous traffic flow considering degradations of connected automated vehicles and reaction time, Phys. A Stat. Mech. Its Appl. 561 (2021), 125218, https://doi.org/10.1016/j.physa.2020.125218.
[36] Z. Yao, Q. Gu, Y. Jiang, B. Ran, Fundamental diagram and stability of mixed traffic flow considering platoon size and intensity of connected automated vehicles, Phys. A Stat. Mech. Its Appl. 604 (2022), 127857, https://doi.org/10.1016/j.physa.2022.127857.
[37] Y. Jiang, S. Sun, F. Zhu, Y. Wu, Z. Yao, A mixed capacity analysis and lane management model considering platoon size and intensity of CAVs, Phys. A Stat. Mech. Its Appl. 615 (2023), 128557, https://doi.org/10.1016/j.physa.2023.128557.
[38] R. Luo, Q. Gu, T. Xu, H. Hao, Z. Yao, Analysis of linear internal stability for mixed traffic flow of connected and automated vehicles considering multiple influencing factors, Phys. A Stat. Mech. Its Appl. 597 (2022), 127211, https://doi.org/10.1016/j.physa.2022.127211.
[39] R.E. Chandler, R. Herman, E.W. Montroll, Traffic dynamics: studies in car following, Oper. Res. 6 (1958) 165–184, https://doi.org/10.1287/opre.6.2.165.
[40] M. Bando, K. Hasebe, K. Nakanishi, A. Nakayama, Analysis of optimal velocity model with explicit delay, Phys. Rev. E - Stat. Physics, Plasmas, Fluids, Relat. Interdiscip. Top. 58 (1998) 5429–5435, https://doi.org/10.1103/PhysRevE.58.5429.
[41] G. Orosz, B. Krauskopf, R.E. Wilson, Bifurcations and multiple traffic jams in a car-following model with reaction-time delay, Phys. Nonlinear Phenom. 211 (2005) 277–293, https://doi.org/10.1016/j.physd.2005.09.004.
[42] D. Ngoduy, Linear stability of a generalized multi-anticipative car following model with time delays, Commun. Nonlinear Sci. Numer. Simul. 22 (2015) 420–426, https://doi.org/10.1016/j.cnsns.2014.08.019.
[43] D. Sun, D. Chen, M. Zhao, W. Liu, L. Zheng, Linear stability and nonlinear analyses of traffic waves for the general nonlinear car-following model with multi-time delays, Phys. A Stat. Mech. Its Appl. 501 (2018) 293–307, https://doi.org/10.1016/j.physa.2018.02.179.
[44] G. Ma, M. Ma, S. Liang, Y. Wang, Y. Zhang, An improved car-following model accounting for the time-delayed velocity difference and backward looking effect, Commun. Nonlinear Sci. Numer. Simul. 85 (2020), https://doi.org/10.1016/j.cnsns.2020.105221.
[45] Y. Jin, M. Xu, Stability analysis in a car-following model with reaction-time delay and delayed feedback control, Phys. A Stat. Mech. Its Appl. 459 (2016) 107–116, https://doi.org/10.1016/j.physa.2016.04.038.
[46] M. Bando, K. Hasebe, A. Nakayama, A. Shibata, Y. Sugiyama, Dynamical model of traffic congestion and numerical simulation, Phys. Rev. E. 51 (1995) 1035–1042, https://doi.org/10.1103/PhysRevE.51.1035.
[47] D. Helbing, B. Tilch, Generalized force model of traffic dynamics, Phys. Rev. E - Stat. Physics, Plasmas, Fluids, Relat. Interdiscip. Top. 58 (1998) 133–138, https://doi.org/10.1103/PhysRevE.58.133.
[48] R. Jiang, Q. Wu, Z. Zhu, Full velocity difference model for a car-following theory, Phys. Rev. E - Stat. Physics, Plasmas, Fluids, Relat. Interdiscip. Top. 64 (2001) 4, https://doi.org/10.1103/PhysRevE.64.017101.
[49] T.S. Komatsu, S.I. Sasa, Kink soliton characterizing traffic congestion, Phys. Rev. E. 52 (1995) 5574–5582, https://doi.org/10.1103/PhysRevE.52.5574.
[50] H.X. Ge, R.J. Cheng, S.Q. Dai, KdV and kink-antikink solitons in car-following models, Phys. A Stat. Mech. Its Appl. 357 (2005) 466–476, https://doi.org/10.1016/j.physa.2005.03.059.
[51] T. Nagatani, Thermodynamic theory for the jamming transition in traffic flow, Phys. Rev. E - Stat. Physics, Plasmas, Fluids, Relat. Interdiscip. Top. 58 (1998) 4271–4276, https://doi.org/10.1103/PhysRevE.58.4271.
[52] T. Nagatani, Density waves in traffic flow, Phys. Rev. E - Stat. Physics, Plasmas, Fluids, Relat. Interdiscip. Top. 61 (2000) 3564–3570, https://doi.org/10.1103/PhysRevE.61.3564.
[53] K. Hussain, F. Ismail, N. Senu, Solving directly special fourth-order ordinary differential equations using Runge-Kutta type method, J. Comput. Appl. Math. 306 (2016) 179–199, https://doi.org/10.1016/j.cam.2016.04.002.